BREAKTHROUGHS IN LOW-PROFILE LEAKY-WAVE HPM ANTENNAS

Prepared by: Sammuel M. Jalali and Robert A. Koslover (PI)

Scientific Applications & Research Associates, Inc.
6300 Gateway Drive
Cypress, CA 90630-4844

21 Dec 2015

Data Item: A002 - Progress, Status, & Management Quarterly Report #9

Prepared for:

Program Officer: Lee Mastroianni
ONR Code 30

OFFICE OF NAVAL RESEARCH
875 North Randolph Street
Suite 1425
Arlington, VA 22203-1995

REPORT DOCUMENTATION PAGE

Form Approved
OMB No. 0704-0188

1. REPORT DATE *(DD-MM-YYYY)*	**2. REPORT TYPE**	**3. DATES COVERED** *(From - To)*
21-12-2015	Quarterly	20 Sep 2015 - 18 Dec 2015

4. TITLE AND SUBTITLE
Breakthroughs in Low-Profile Leaky-Wave HPM Antennas
Progress, Status, & Management Report
(Quarterly Report #9)

5a. CONTRACT NUMBER
N00014-13-C-0352

5b. GRANT NUMBER

5c. PROGRAM ELEMENT NUMBER

6. AUTHOR(S)
Jalali, Sammuel M., and Koslover, Robert A.

5d. PROJECT NUMBER

5e. TASK NUMBER

5f. WORK UNIT NUMBER

7. PERFORMING ORGANIZATION NAME(S) AND ADDRESS(ES)

Scientific Applications &
Research Associates, Inc.
6300 Gateway Drive
Cypress, CA 90630-4844

8. PERFORMING ORGANIZATION REPORT NUMBER

9. SPONSORING / MONITORING AGENCY NAME(S) AND ADDRESS(ES)
Office of Naval Research
875 North Randolph Street
Suite 1425
Arlington, VA 22203-1995

10. SPONSOR/MONITOR'S ACRONYM(S)
Code 30

11. SPONSOR/MONITOR'S REPORT NUMBER(S)

12. DISTRIBUTION / AVAILABILITY STATEMENT
Distribution Statement A. Approved for public release; distribution is unlimited. Other requests for this document shall be referred to the Program Officer listed in the contract.

13. SUPPLEMENTARY NOTES
..

14. ABSTRACT
This report describes progress during the 9th quarter of this program and highlights the current status of the research. Technical activities this period emphasized a generalization of the plane-wave decomposition approach (used previously to guide initial FAWSEA design recipes) to apply to the Arched Aperture Waveguide Sidewall-Emitting Antenna (AAWSEA). The resulting expressions form a basis for developing more general design scripts, which should allow us to account for (and at least partially compensate for) H-plane aperture curvature prior to the use of computationally-intensive numerical modeling for design optimization.

15. SUBJECT TERMS
Leaky-wave Antennas. High Power Microwaves (HPM) Antennas. Low-profile Conformal Antennas.

16. SECURITY CLASSIFICATION OF:			**17. LIMITATION OF ABSTRACT**	**18. NUMBER OF PAGES**	**19a. NAME OF RESPONSIBLE PERSON (Monitor)**
a. REPORT	**b. ABSTRACT**	**c. THIS PAGE**			Lee Mastroianni
Unclassified	Unclassified	Unclassified	SAR	___	**19b. TELEPHONE NUMBER**(incl. area code) (703) 696-3073

Standard Form 298 (Rev. 8-98)
Prescribed by ANSI Std. Z39.18

Table of Contents

List of Figures

1. INTRODUCTION

This is SARA's 9h Quarterly Report for "Breakthroughs in Low-profile Leaky-Wave HPM Antennas," a 37-month Basic Research effort sponsored by the US Office of Naval Research (ONR). This work includes fundamental theoretical analyses, numerical modeling, and related basic research. Objectives include to discover, identify, investigate, characterize, quantify, and document the performance, behavior, and design of innovative High Power Microwave (HPM, GW-class) antennas of the *forward-traveling*, *fast-wave*, *leaky-wave* class.

1.1. Overview of Previous Activities (1st thru 8th Quarter)

During the *first* quarter, we prepared and established useful equations and algorithms for predicting reflections and transmission of incident TE waves from parallel-wire grills, dielectric windows, and combinations of wire grills with dielectric windows, in problems reducible to purely H-plane (2D) representations. We then applied this theory to guide the design of high-gain configurations (again, limited to 2D, H-plane representations) for linear, forward traveling-wave, leaky-wave antennas. The theory built upon equivalent circuit methods and wave matrix theory, which provided useful formalisms upon which we continue to build.

During the *second* quarter, we pursued initial extensions of the previous work into three dimensions, in order to include phenomena with E-plane dependencies. We succeeded in adding into the wave-matrix formalism the reflection/transmission properties associated with the transition to free space from a *finite-width* leaky-wave channel, including the edge-tapering essential to HPM applications. These geometric aspects do not arise in analyses confined to the H-plane alone. Our 3D analyses were somewhat more reliant on numerical models than in the 2D analyses, due to the greater complexity of identifying and/or building practical analytic approaches capable of addressing true 3D geometries of interest.

During the *third* quarter, we explored channel-to-channel coupling (aka, mutual coupling) which (as we have noted earlier) is an important design concern, since it can impact antenna performance significantly in terms of gain, peak power-handling, and impedance matching. Our approach leveraged mostly numerical methods, along with some intuitive arguments, as we explored designs exhibiting different degrees of mutual coupling between adjacent channels. As past and current antenna literature attest, mutual coupling analyses are non-trivial; suffice to say, there is still much work to be done in this area.

During the *fourth* quarter, we continued to study and employ wave-matrix based methods, but with less success than before in applying this approach to *improve* or *optimize* the initial designs. The formalism itself is still valid, but offers reduced practical rewards once an *initial* (i.e., not fully-optimized) geometry (e.g., grill, window, channel depth, etc.) is derived from the more basic-level principles. At that stage, we are finding that further optimization is currently best proceeding via numerical means. Additional work in the fourth quarter led us to identify *new aperture geometries* of potentially-significant practical value, which included the "BAWSEA" and "GAWSEA". These configurations may significantly extend the utility of leaky-wave antenna technology to support integration on more challenging platforms.

During the *fifth* quarter, we designed, analyzed, and documented representative high-performance FAWSEA and CAWSEA antennas suitable for designation as "standard" or "recommended." The configurations we described were scalable with wavelength. These are the initial entries in a library of antennas that will continue to be built throughout this program.

During the *sixth* quarter, we performed additional investigation of designs to support the newer curved apertures, especially the "Bent Aperture Waveguide Sidewall-emitting Antenna" (BAWSEA). We presented this work at the 17th Annual Directed Energy Professional Society (DEPS) Symposium in Anaheim, CA, on March 4th, 2015. Our full slide presentation, entitled "Advances in Low-Profile Leaky-Wave Conformable Antennas for HPM Applications," was included in the unclassified proceedings CD that was recently distributed by DEPS to all the conference attendees.

During the *seventh* quarter, we investigated RAWSEA design considerations and showed that the angle of rotation between the leaky wave channels and the aperture can be understood in terms of an equivalent linear (non-rotated) displacement, an interpretation which helps to guide application of the wave-matrix formalism. However, more work is still needed to speed-up the RAWSEA design process.

During the *eighth* quarter, we identified, investigated, and applied a seemingly-simple but clarifying wave-mapping methodology, which provided improved guidance in making optimal use of generally curved platform surfaces. Following this process helps guide the designer toward a solution that provides both higher gain and greater peak power handling. Via this approach we identified and reported a notable success with the design of an improved CAWSEA that can deliver superior gain, yet still conform to the same radius cylinder as our earlier-suggested "standard/recommended" design.

For more information, we encourage the reader to refer our earlier *Quarterly Reports #1* thru *#8.*

1.2. Overview of Recent Activities (9th Quarter)

Most of the technical work for the 9th quarter was performed by SARA Staff Scientist Dr. Sammuel M. Jalali. In particular, the PI (Dr. Koslover) asked Dr. Jalali to investigate and document a theoretical framework/toolset to help guide the AAWSEA[1] design process, in analogy to the theory and tools we documented in earlier reports that already guide the design of new FAWSEAs and CAWSEAs. To that end, Dr. Jalali sought to expand the applicability of plane-wave decomposition (see our 1st Quarterly Report) into a more general, but also inherently more-approximate, ray-tracing technique. This approach employs an analytic parameterization of the inner-curve (channel back-wall) and outer-curve (vicinity of the leaky-grill wall) ogives, while tracking the varying angles of reflection sequentially along the perspective leaky guide, and ultimately adjusting these curves to yield the desired output beam. In principle, this kind of approach should work, given *sufficiently-gradual* curvature. At this stage, it at least offers some insight. More work is needed to advance this analysis, to integrate it into the framework we previously reported, and to establish whether it is actually useful in the generation of practical design recipes for efficient, high-gain, high-P_{pk} capable, AAWSEA configurations.

Further information about the aforementioned research is provided in Section 3.

1.3. Upcoming conferences

The DEPS 18th Annual Directed Energy Symposium, will be held in Albuquerque, NM, March 7-11, 2016. The Call For Papers is posted at http://www.deps.org/DEPSpages/DEsymp16.html, with abstracts due Jan 8, 2016. We would like to attend this important conference and present an update to the DEW community, summarizing the current status of the research and progress made since last year. Since the abstract deadline is now rapidly approaching, we will prepare an abstract for review by ONR very shortly.

In addition, we note that there is also an IEEE AP-S/USNC-URSI conference to be held June 25-July 1, 2016, in Puerto Rico (see http://www.2016apsursi.org/CallForPapers.asp). The paper submission deadline for that conference is also relatively soon (Jan. 18, 2016). We solicit ONR's guidance in regard to the value of our attending and presenting this work to the wider-community at the IEEE AP-S/USNC-URSI conference.

[1] Recall that the AAWSEA, or "Arched Aperture Waveguide Sidewall-Emitting Antenna," specifically denotes a configuration with aperture-curvature in the H-plane. A list of acronyms we have used to date for variously flat and curved-surface leaky-wave antennas may be found in *Table 1* of the *4th Quarterly Repor*t, Sept. 18, 2014.

2. STATUS OF THE PLAN/SCHEDULE AND FUNDING

Figure 1 (next page) maps out the updated program plan, for quick reference. The subject contract was awarded on 9/18/2013 and has an end date of 10/17/2016. The total contract value is $868,350, with current (per P00005 signed on 3/17/2015) authorized funding of $780,473. According to SARA's accounting system, as of Dec. 11, 2015, expenses and commitments (including fee) totaled $595,502, thus leaving $184,971 available, as of that date. If one simply compares the calendar and spending on this project, we have consumed 71.8% of the calendar, 68.6% of the total contract value, and 76.3% of the authorized funds. We thank ONR for the continued support of this project.

As the observant reader may have noted, some of the R&D paths in this program have shifted as we have gradually identified and pursued many interesting antenna questions and novel design opportunities within the family of low-profile, high-power-capable, forward-traveling, leaky-wave antennas. This has led to some schedule slippage of the planned optimized-design milestones in Task 3, so we will now need to focus more closely upon completing those tasks. Overall, there are no significant technical, schedule, or funding-related program problems to report at this time.

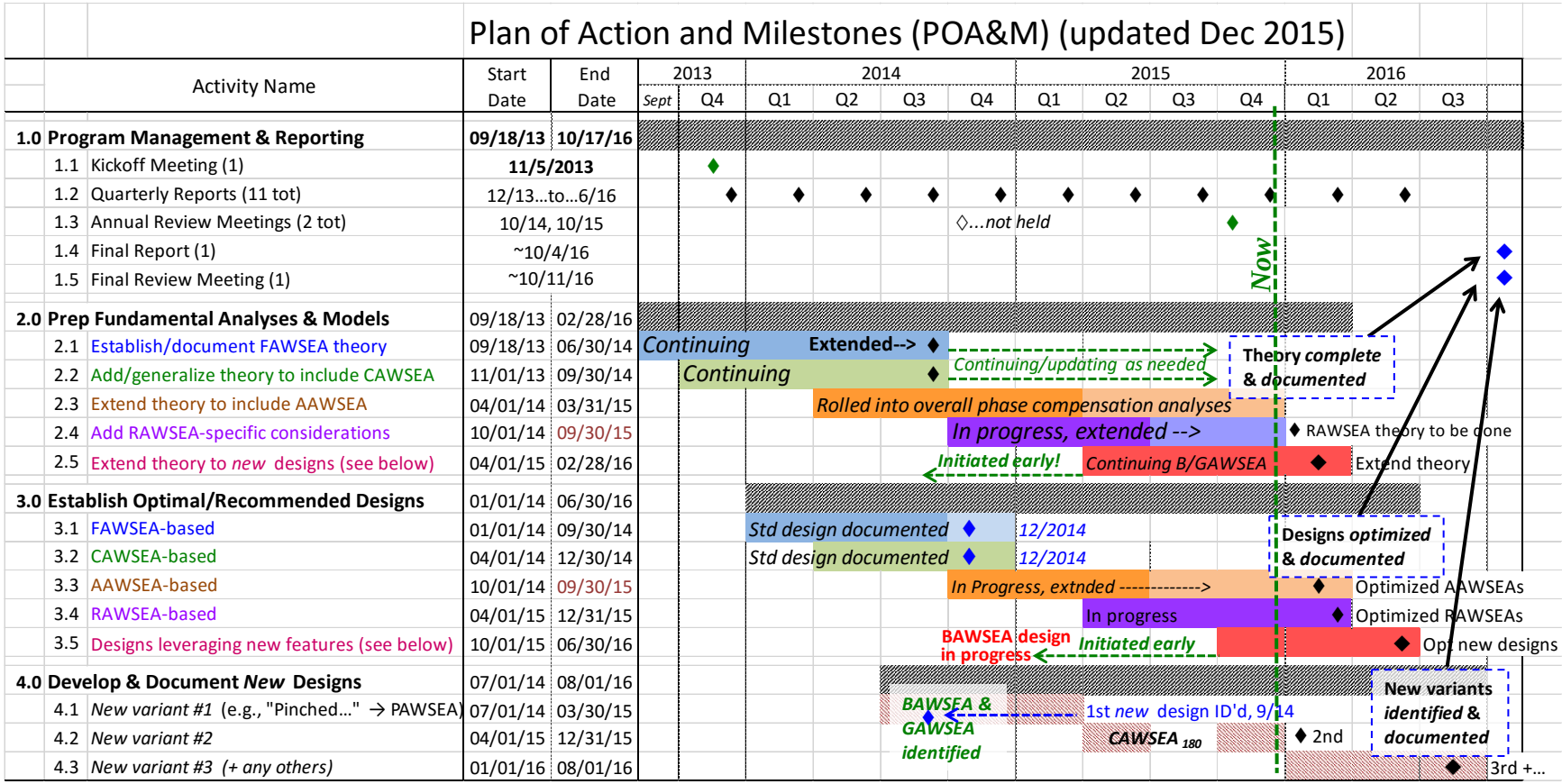

Figure 1. Updated Program Plan

3. RESEARCH AND ACTIVITIES PERFORMED THIS PERIOD

3.1. Generalization of plane-wave wave-decomposition to AAWSEA analyses

We consider the basic analysis of an AAWSEA below. This configuration is an important one, representative of constraints of payloads and the common necessity of conformal matching of the antenna aperture to a potential DEW platform. The first part below is intended to investigate the possibility of mathematical analysis and development of an algorithm to compensate for the phase velocity changes and radiated plane wave disturbance caused by the arched (i.e., curved in the H-plane) structure. A simplified model with no dielectric window is considered throughout. In leaky-wave antenna (LWA) structures with *flat* side walls (whether leaky or conducting walls) such as the FAWSEA, plane waves are radiated at an angle relative to end-fire approximately equal to the complement of $\theta_o = \cos^{-1}\left(\frac{f_c}{f}\right)$ with f_C being the effective cut-off frequency of the guide and f being the operating frequency. In such structures, the guided phase velocity is constant along the device through the relation of $v_p = \left(\frac{\lambda_g}{\lambda_o}\right)c$, where λ_g is the guided wavelength and λ_o is the free-space wavelength. For the purpose of analysis the guided wave can be decomposed in two interfering TEM plane-waves reflecting from side walls. These TEM waves provide a convenient tool for demonstration and analysis of the propagating waves. One of these waves is shown in Figure 2 in addition to the geometric relations between free-space and phase velocities.

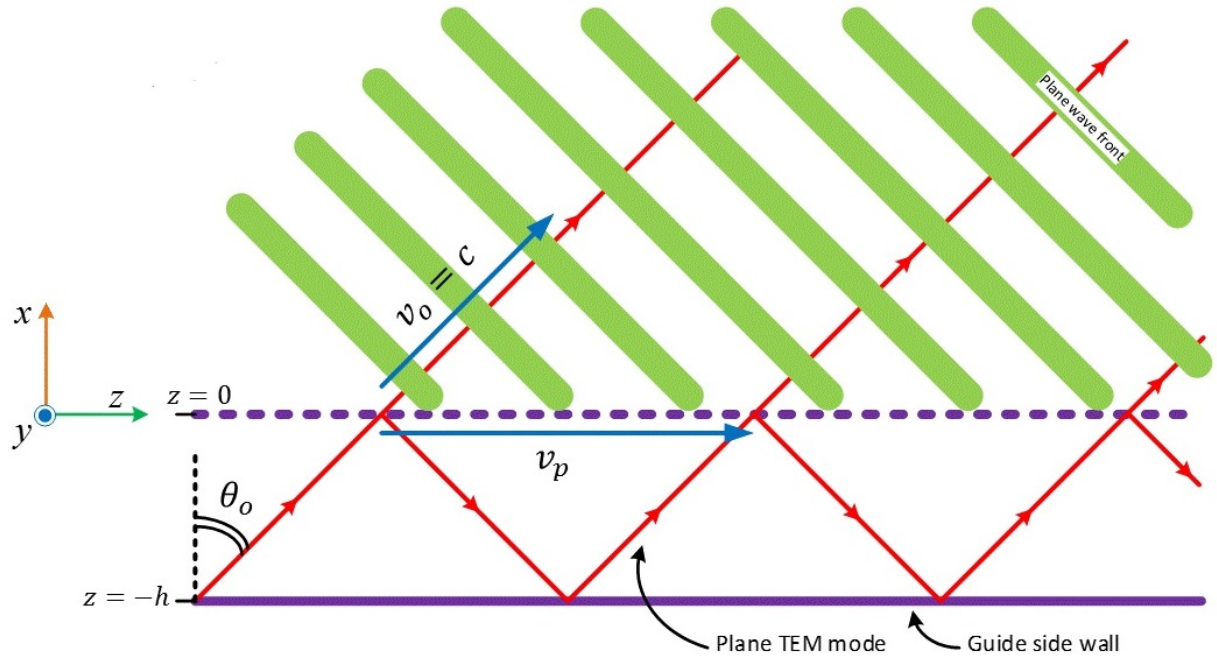

Figure 2. Plane-wave representation of waveguide mode.

When the side walls are arched, the phase velocity changes along the guide and consequently plane wave radiation matching that of the case with flat guide walls no longer occurs. This result is consistent with the simple plane-wave decomposition in Figure 3. In this figure, both walls are bent similarly (that is, the same curve is used for both side walls). As can be seen from the figure, the wave direction is altered and therefore the geometry needs to be modified to achieve a proper plane-wave output radiation.

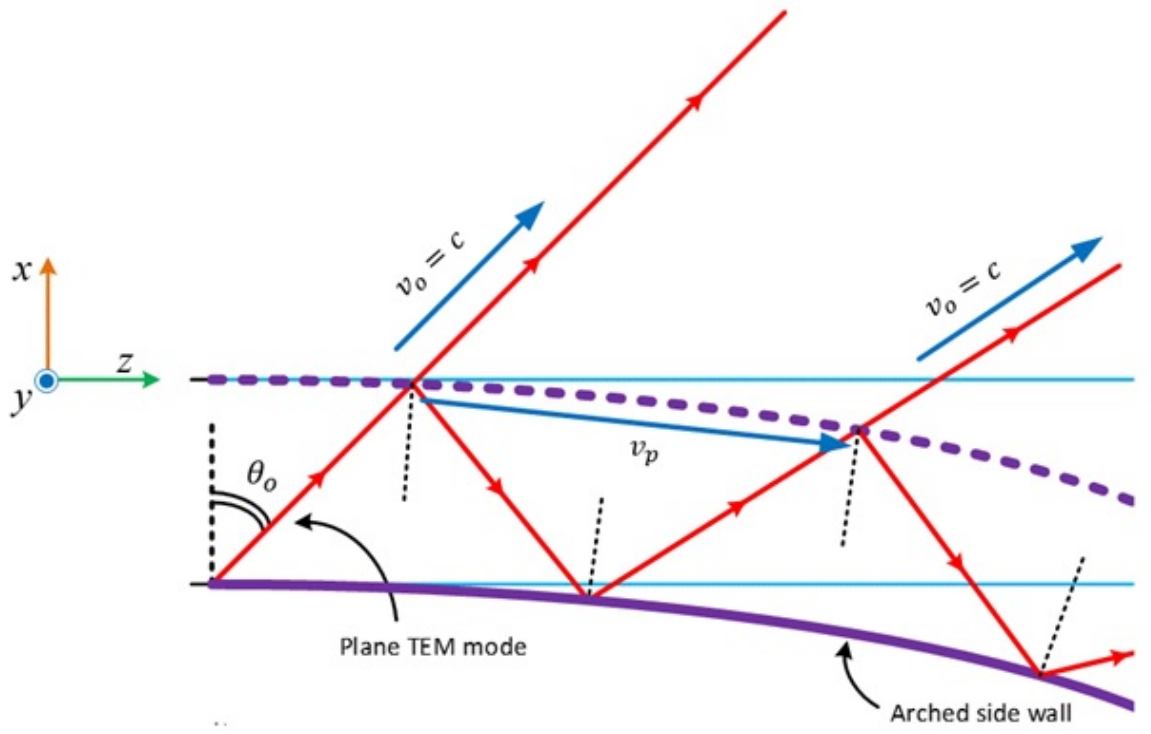

Figure 3. Plane-wave view of wave propagation around an arch (H-plane curve).

3.2. Simulating the guide with parallel side walls

Let's first mathematically formulate the process for the LWA with *similarly* arched side walls in order to demonstrate the existing problem and verify the prediction made in Figure 3. Although an arch with a true ogive shape is desirable, we will use a simpler curve equation to ease our initial simulation. (Ogive curves are studied in a later section.) The complete simulation is written in Matlab script that can be simply modified for other choices of curves. Let us assume a simple quadratic curve for both side walls (leaky and PEC), that is

$$f(z) = -C_1 z^2 \text{ and } g(z) = -C_2 z^2 - h \quad (1)$$

We choose a small, positive, and equal value for the quadratic coefficients $C_1 = C_2$ and h is the wave guide width. From basic waveguide relations we have the cutoff frequency $f_C = \frac{c}{2h}$. We also choose an appropriate operating frequency f from which the radiation angle is computed by $90^o - \theta_o = 90^o - \cos^{-1}\left(\frac{f_C}{f}\right)$.

For mathematical analysis we only include one of the plane waves. Obviously the other TEM wave will be treated similarly. Figure 4 shows the first partial reflection of the TEM wave from the leaky side wall.

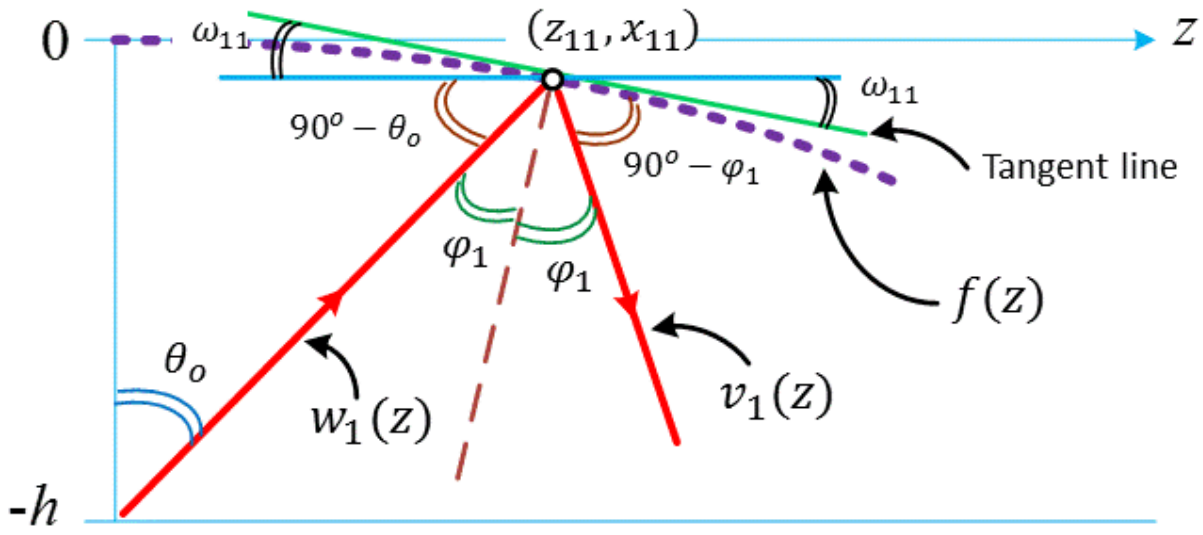

Figure 4. First reflection from (idealized) curved wall.

First we determine the equation for the ray $w_1(z)$ that passes through the point $(z = 0\,, x = -h)$ with the slope of

$$m_{w_1} = \tan(90^o - \theta_o) = \cot\theta_o \qquad (2)$$

$$w_1(z) = (\cot\theta_o)z - h \qquad (3)$$

The intersection of this line and the upper side wall that is the intersection of $f(z)$ and $w_1(z)$ is computed to obtain the point (z_{11}, x_{11}).

$$f(z) = w_1(z) \rightarrow C_1 z^2 + (\cot\theta_o)z - h = 0 \qquad (4)$$

The roots are

$$z = -\frac{\cot\theta_o}{2C_1} \pm \frac{\sqrt{\cot^2\theta_o + 4C_1 h}}{2C_1} \qquad (5)$$

Here we must select the positive root of $z_{11} = -\frac{\cot\theta_o}{2C_1} + \frac{\sqrt{\cot^2\theta_o + 4C_1 h}}{2C_1}$. Notice that because $\sqrt{\cot^2\theta_o + 4C_1 h} > \cot\theta_o$ the existence of the positive root is guaranteed. Having this intersection point we can find the absolute slope angle of the upper side wall.

$$\omega_{11} = |\tan^{-1}(f'(z_{11}))| = |\tan^{-1}(-2C_1 z_{11})| = \tan^{-1}(2C_1 z_{11})$$

Now we find the equation for the reflected ray $v_1(z)$. The slope is computed as follows (see Figure 5).

$$m_{v_1} = -\tan(\theta_2) = -\tan\big(\omega_{11} + (90^o - \varphi_1)\big)$$

$$\varphi_1 = 90^o - (90^o - \theta_o) - \omega_{11} = \theta_o - \omega_{11}$$

$$m_{v_1} = -\tan(90^o - \theta_o + 2\omega_{11}) = -\cot(\theta_o - 2\omega_{11}) \qquad (6)$$

The ray $v_1(z)$ also passes through the point (z_{11}, x_{11}) and therefore the line equation can be written using (6).

$$v_1(z) = m_{v_1}(z - z_{11}) + x_{11} = -\cot(\theta_o - 2\omega_{11})\,z + x_{11} + \cot(\theta_o - 2\omega_{11})\,z_{11} \qquad (7)$$

Now equipped with the equation of the ray $v_1(z)$ and the lower side wall equation $g(z)$ we find the intersection point (z_{12}, x_{12}) shown in Figure 5.

$$g(z) = v_1(z) \rightarrow -C_2 z^2 - h = -\cot(\theta_o - 2\omega_{11})\, z + x_{11} + \cot(\theta_o - 2\omega_{11})\, z_{11} \quad (8)$$

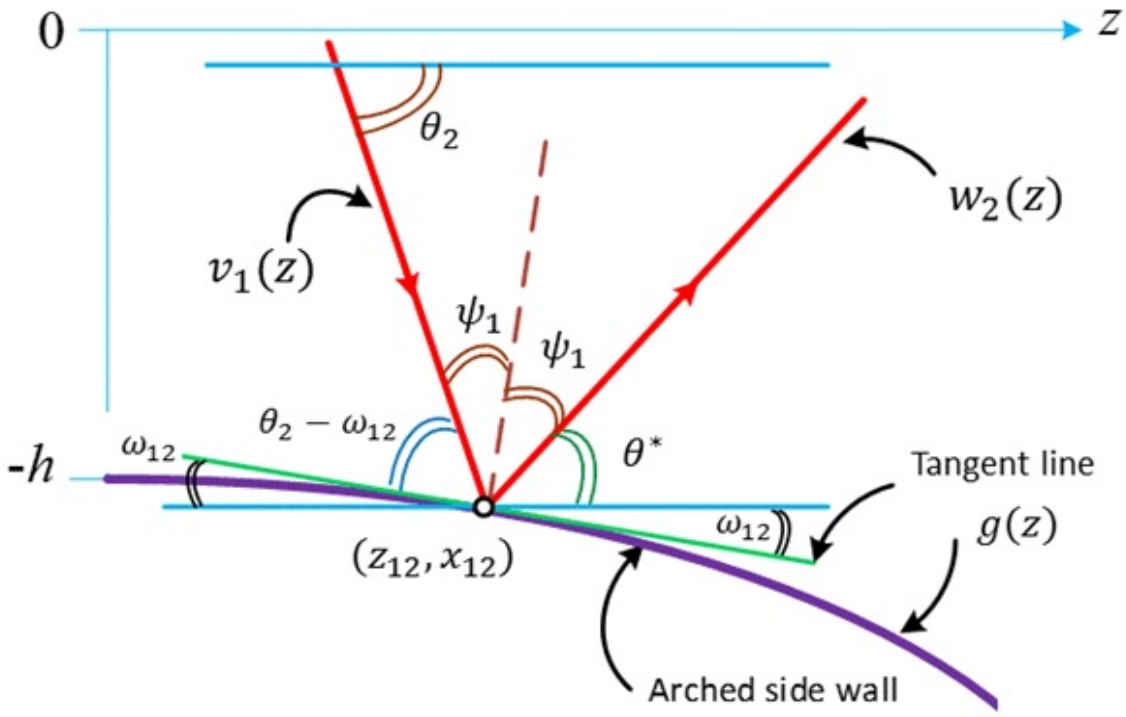

Figure 5. Next reflection, from (idealized) curved wall.

Equation (8) leads to another quadratic equation that is being solved to find the intersection point (z_{12}, x_{12}).

$$C_2 z^2 - \cot(\theta_o - 2\omega_{11})\, z + [h + x_{11} + \cot(\theta_o - 2\omega_{11})\, z_{11}] = 0 \quad (9)$$

Equation (9) has two roots with at least one positive (with the similar justification as for equation (4)). Let us denote this root by z_{12} from which the $x_{12} = g(z_{12}) = -C_2 z_{12}^2 - h$ is computed. This point can be used to find the absolute slope angle of the lower side wall, per Figure 5.

$$\omega_{12} = |\tan^{-1}(g'(z_{12}))| = |\tan^{-1}(-2C_2 z_{12})| = \tan^{-1}(2C_2 z_{12})$$

Also notice that the angle θ_2 is known from the slope of $w_1(z)$ in previous step.

$$\theta_2 = 90^o - \theta_o + 2\omega_{11}$$

$$\psi_1 = 90^o - (\theta_2 - \omega_{12}) = 90^o - \theta_2 + \omega_{12} = \theta_o - 2\omega_{11} + \omega_{12}$$

The critical angle that also specifies the slope of the reflected ray $w_2(z)$ in Figure 4 is denoted by θ^* and is found by the following.

$$\theta^* = 90^o - \psi_1 - \omega_{12} = 90^o - \theta_o + 2\omega_{11} - 2\omega_{12} \quad (10)$$

Now the equation for the third reflected ray can be computed using the slope angle θ^* and the intersection point (z_{12}, x_{12}).

$$w_2(z) = m_{w_2}(z - z_{12}) + x_{12}$$

$$m_{w_2} = \tan(\theta^*) = \tan(90^o - \theta_o + 2\omega_{11} - 2\omega_{12}) = \cot(\theta_o - 2\omega_{11} + 2\omega_{12})$$

$$w_2(z) = \cot(\theta_o - 2\omega_{11} + 2\omega_{12})\, z + [x_{12} - \cot(\theta_o - 2\omega_{11} + 2\omega_{12})\, z_{12}] \quad (11)$$

Finally this process can be carried on for as many reflections as there are in the guide length not only for the plane wave shown in the above but also for the complementary plane wave that starts from the top side wall.

We have prepared a Matlab script (included here, for convenient reference) to perform these operations and plot the implied radiated rays, to visualize the problem that arises from variation of the phase velocity in an arched leaky wave guide. The parameters used are: $h = 0.1651$ m, $L = 1.0$ m, and $f = 1$ GHz.

```
% Script name: "Vp_test1.m"  (C:\Matlab\NAV41)
% This script is used to demonstrate the effect of arched guide on the
% phase velocity and on the radiated plain wave.
%
%  Sam Jalali, SARA, Inc., Cypress, California
%  Version: 1.0,  10/30/2015
% ************************************************************************
close all; clear all;
format long; format compact;

c_const = 2.99792458e8;
L = 1.0;         % guide length in meters
h = 165.1e-3;    % guide width in meters
C1 = 0.10;       % upper side wall equation f(z) = -C1*z^2
C2 = C1;         % lower side wall equation g(z) = -C2*z^2-h
fc = c_const/(2*h);   % cutoff fequency in GHz
f = 1.0e9;            % operating frequency
Tets = acos(fc/f);    % TEM modes angle
% Draw the upper and lower side walls of the guide
z=linspace(0,L,500);
for n = 1:length(z)
    X1(n) = -C1*z(n)^2;     % upper sidewall (grid) equation
    X2(n) = -C2*z(n)^2-h;   % lower sidewall equation
end
plot(z,X1,':k','LineWidth',3.5); hold on;
plot(z,X2,'-k','LineWidth',3.0); grid on;
xlabel('z','FontSize',18,'FontWeight','bold','Color','b','FontAngle',...
    'italic','FontName','Times New Roman');
ylabel('x','FontSize',18,'FontWeight','bold','Color','b','FontAngle',...
    'italic','FontName','Times New Roman');
title('TEM mode decomposition','FontSize',14,'FontWeight','bold',...
    'Color','b','FontName','Times New Roman');

N = 7;                      % number of reflections in the guide
% Start of the loop (N iterations), for lower TEM mode ray
zo = 0; Ko = -h; Tet0 = Tets;
for n=1:N
    % Compute the intersection of w1(z) with upper side wall
    m1 = cot(Tet0);          % slope of w1(z)
    ZR = roots([C1,m1,Ko-m1*zo]);
    z1 = ZR(2);
    if z1 <= 0
        error('The z vale is negative');
    end
    x1 = -C1*z1^2;
    % Draw the ray section w1(z)
    XL = 1.0;                % top X limit for plane wave
    ZL = (XL-Ko+m1*zo)/m1;   % corresponding Z limit
    if ZL >= L
```

```
        ZL = L;
    end
    z = linspace(zo,ZL,300);
    for n = 1:length(z)
        w1(n) = m1*z(n)+Ko-m1*zo;
    end
    plot(z,w1,'-r','LineWidth',3.0);
    % Compute the next ray section
    Tet1 = abs(atan(-2*C1*z1));       % w1(z) slope angle absolute value
    % Phi1 = Tet0-Tet1; Phi2 = pi/2-Phi1+Tet1;
    Phi2 = pi/2-Tet0+2*Tet1;   % angle of w2(z) in absolute value
    % Compute the intersection of w2(z) with lower side wall
    m2 = -tan(Phi2);           % slope of w2(z)
    K1 = h+x1-m2*z1;
    ZR = roots([C2,m2,K1]);
    z2 = ZR(2);
    if (z2 <= 0)
        error('The z vale is negative');
    end
    x2 = -C2*z2^2-h;
    % Draw the ray section w2(z)
    z = linspace(z1,z2,300);
    for n = 1:length(z)
        w2(n) = m2*z(n)+x1-m2*z1;    % (z2,x2) could've been used too
    end
    plot(z,w2,'-r','LineWidth',3.0);
    % Prepare the parameters for next iteration
    Tet2 = abs(atan(-2*C2*z2));      % w2(z) slope angle absolute value
    % Psi = pi/2-Phi2+Tet2; Tets = pi/2-Psi-Tet2;
    Tetc = pi/2-Tet0+2*Tet1-2*Tet2;  % the crtical angle
    Tet0 = pi/2-Tetc;                % New TEM angle
    zo = z2; Ko = x2;
end

% Start of the loop (N iterations), for upper TEM mode ray
zo = 0; Ko = 0; Tet0 = Tets;
for n=1:N
    % Compute the intersection of w1(z) with upper side wall
    m1 = -cot(Tet0);           % slope of w1(z)
    ZR = roots([C2,m1,Ko-m1*zo+h]);
    z1 = ZR(2);
    if z1 <= 0
        error('The z vale is negative');
    end
    x1 = -C2*z1^2-h;
    % Draw the ray section w1(z)
    z = linspace(zo,z1,300);
    for n = 1:length(z)
        w1(n) = m1*z(n)+Ko-m1*zo;
    end
    plot(z,w1,'-m','LineWidth',3.0);
    % Compute the next ray section
    Tet1 = abs(atan(-2*C2*z1));
    % Phi1 = pi/2-Tet0; Phi2 = pi/2-Phi1+Tet1;
    Tetc = pi/2-Tet0-2*Tet1;   % angle of w2(z) in absolute value, criitical
    % Compute the intersection of w2(z) with lower side wall
    m2 = tan(Tetc);
    K1 = x1-m2*z1;
    ZR = roots([C1,m2,K1]);
    z2 = ZR(2);
    if (z2 <= 0)
        error('The z vale is negative');
    end
    x2 = -C1*z2^2;
    % Draw the ray section w2(z)
    XL = 1.0;                  % top X limit for plane wave
    ZL = (XL-K1)/m2;    % corresponding Z limit
    if ZL >= L
        ZL = L;
    end
    z = linspace(z1,ZL,300);
```

```
    for n = 1:length(z)
        w2(n) = m2*z(n)+x1-m2*z1;    % (z2,x2) could've been used too
    end
    plot(z,w2,'-m','LineWidth',3.0);
    % Prepare the parameters for next iteration
    Tet2 = abs(atan(-2*C1*z2));       % w1(z) slope angle absolute value
    Tet0 = pi/2-Tetc-2*Tet2;          % New TEM angle
    zo = z2; Ko = x2;
end
```

Figure 6 shows the result of executing the above Matlab script. As can be seen, some compensating technique is required to return the rays to parallel. And that means an adjustment to the phase velocity, as expected, is necessary.

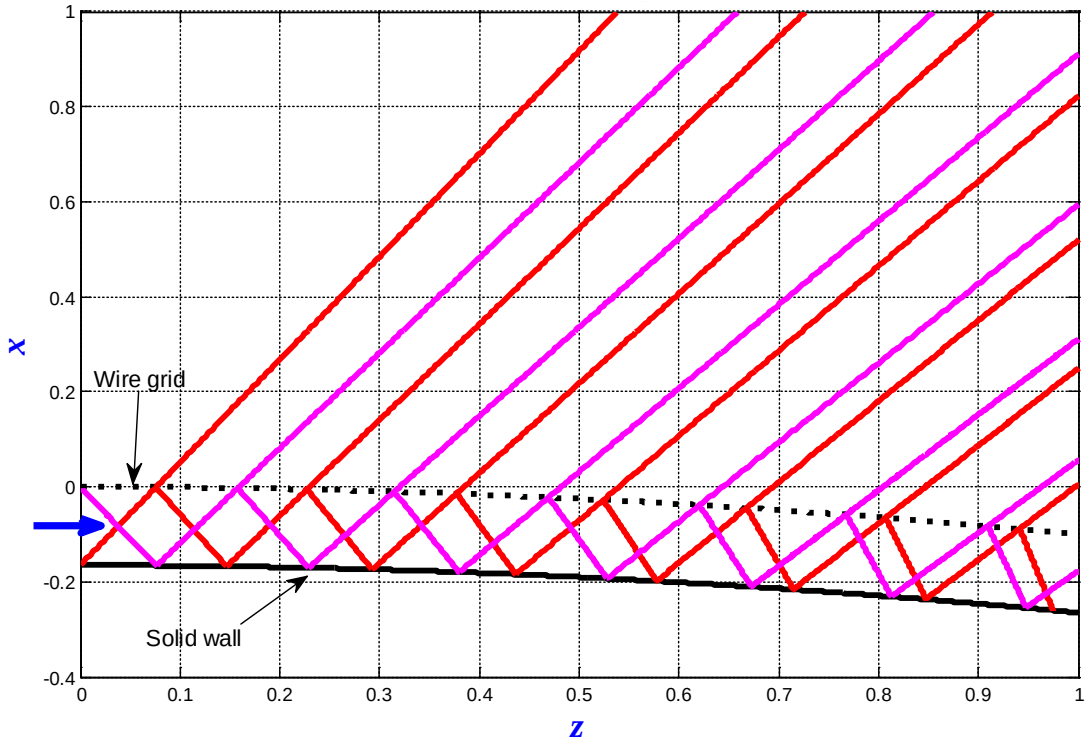

Figure 6. Departure from parallel-ray outputs due to the curved walls.

3.3. Finding the side wall equation for proper phase velocity compensation

The above procedure was based on two simplifying assumptions. First the leaky wall shape was considered to be a simple quadratic, which for practical reasons might be changed to ogive or Bezier shapes. Second, the lower PEC wall was assumed to be known and parallel to the leaky wall (same equation with an offset). In fact, the lower PEC wall should actually be computed for the proper compensation.

Here we retain the same simple curvature for both the leaky wall and the PEC wall to develop the methodology in a simple way. Generalization of the methodology will be discussed later. Therefore, once again we assume the leaky wall to have the equation $f(z) = -C_1 z^2$ and the lower side wall have the same simple quadratic equation $g(z) = -C_2 z^2 - h$. However this time $C_2 \neq C_1$ and in fact we need to compute the appropriate value for C_2 (if possible).

Refer again to Figure 5. For proper operation we require that the reflected ray $w_2(z)$ be in parallel with the first ray in Figure 4 that is $w_1(z)$ and similarly towards the end of the guide. Such requirement mandates that the slope angle of $w_2(z)$ that is θ^* be equal to the slope angle of $w_1(z)$ that is $90^o - \theta_o$. In fact, this was the reason we called θ^* the critical angle.

Now we will proceed to show how the previous requirement leads to a method of finding the proper value of C_2 that determines the shape of lower compensating wall. We have the critical angle value from $\theta^* = 90^o - \theta_o$. From equation (10) in previous section we proceed to find the slope of the tangent line to the lower PEC wall ω_{12} at the point of intersection (z_{12}, x_{12}) that is yet to be determined in this case.

$$\theta^* = 90^o - \theta_o = 90^o - \theta_o + 2\omega_{11} - 2\omega_{12} \quad (10)$$

So the value for this angle can be computed to be equal to the known angle ω_{11} in the following equation

$$\omega_{12} = \omega_{11} \quad (12)$$

We also know from the slope of the tangent line to the lower side wall with $g(z) = -C_2 z^2 - h$ that

$$\omega_{12} = |\tan^{-1}(g'(z_{12}))| = |\tan^{-1}(-2C_2 z_{12})| = \omega_{11} \quad (13)$$

From the equation (13) we can compute the intersection point z_{12} in terms of the unknown coefficient C_2 by taking "tan" of the both sides as follows.

$$2C_2 z_{12} = \tan(\omega_{11}) \rightarrow z_{12} = \frac{\tan(\omega_{11})}{2C_2} \quad (14)$$

But this value of z_{12} must satisfy the equation (9) as follows.

$$C_2 z_{12}^2 - \cot(\theta_o - 2\omega_{11})\, z_{12} + [h + x_{11} + \cot(\theta_o - 2\omega_{11})\, z_{11}] = 0 \quad (15)$$

Inserting equation (14) into (15) we can compute C_2 as follows.

$$C_2 = \frac{\tan(\omega_{11})\,[2\cot(\theta_o - 2\omega_{11}) - \tan(\omega_{11})]}{4[x_{11} + h + \cot(\theta_o - 2\omega_{11})\, z_{11}]} \quad (16)$$

The above procedure demonstrate a general methodology used to determine the geometrical aspects of the lower wall of the LWA to compensate for phase velocity variation in AAWSEA. It also indicates the complications involved in the design of an arched aperture vs. a flat one.
In the general case, one can use this technique to find several computed points for the lower PEC side wall. Although the number of computed points is limited, an interpolation of these points gives an equation in terms of polynomial that can be a good approximation for the target compensating curve.

A modified Matlab script (Vp_Test2.m) is used to demonstrate the result of this methodology. Figure 7 shows the correction made only by computing one compensation point on the lower PEC wall. Obviously, the compensation must be performed for many points (or more generally, a continuum) along the guide. An appropriate analytic function or a high-order polynomial can likely be employed for satisfactory results. We will discuss the latter in the next section.

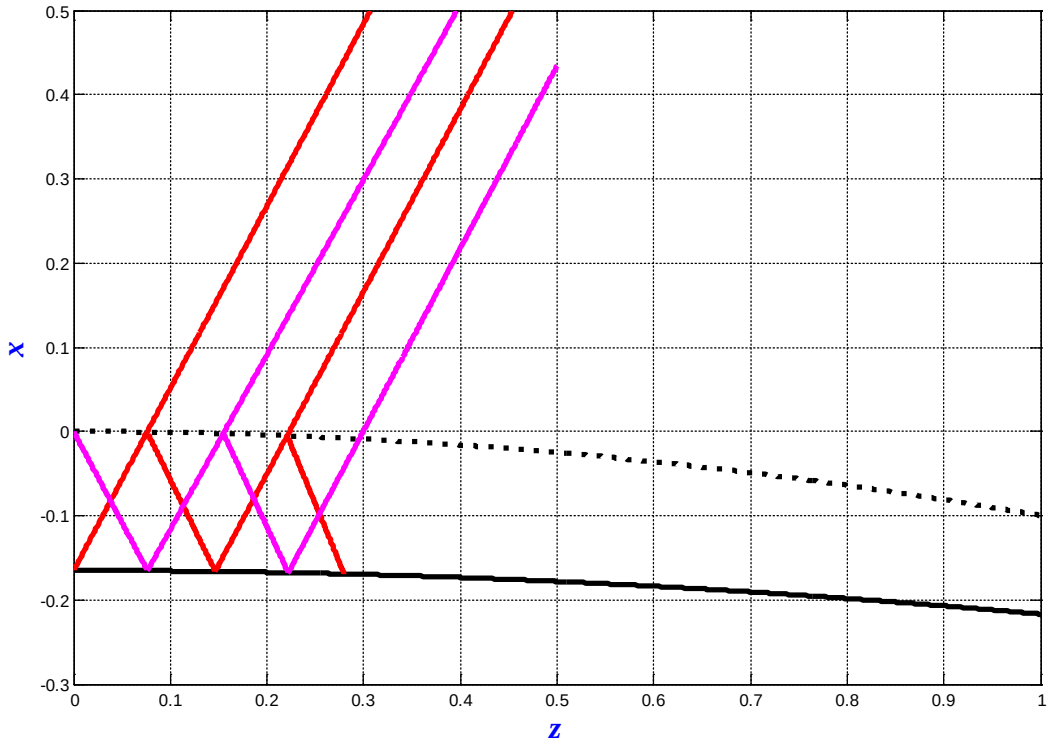

Figure 7. Employing initial phase-velocity compensation.

3.4. Ogive curvature and practical restrictions

Use of ogive curves is common in minimizing the drag caused by air resistance. We will consider the tangent ogive curve given by the following mathematical formula written for our previously used coordinate system.

$$f(z) = \sqrt{\left(d\left(C^2 + \frac{1}{4}\right)\right)^2 - z^2} - d\left(C^2 - \frac{1}{4}\right)$$

In this formula, d is the curvature diameter and $C = \frac{L}{d}$ is called the caliber. Such an ogive curve has an offset of $f(0) = \frac{d}{2}$. In order to match the curve with our upper side wall with no offset of leaky guide ($f(0) = 0$) we modify and simplify the formula to the following:

$$f(z) = \sqrt{\left(d\left(C^2 + \frac{1}{4}\right)\right)^2 - z^2} - d\left(C^2 + \frac{1}{4}\right) = \sqrt{a^2 - z^2} - a \quad (17)$$

The main parameter in the above ogive curve is $a = d\left(C^2 + \frac{1}{4}\right)$. The methodology for compensating phase velocity via the geometric optics technique (used in previous sections) needs to be performed iteratively for multiple reflections. Figure 8 is an extension of Figure 4 and Figure 5. It is used here to clarify the detailed procedure.

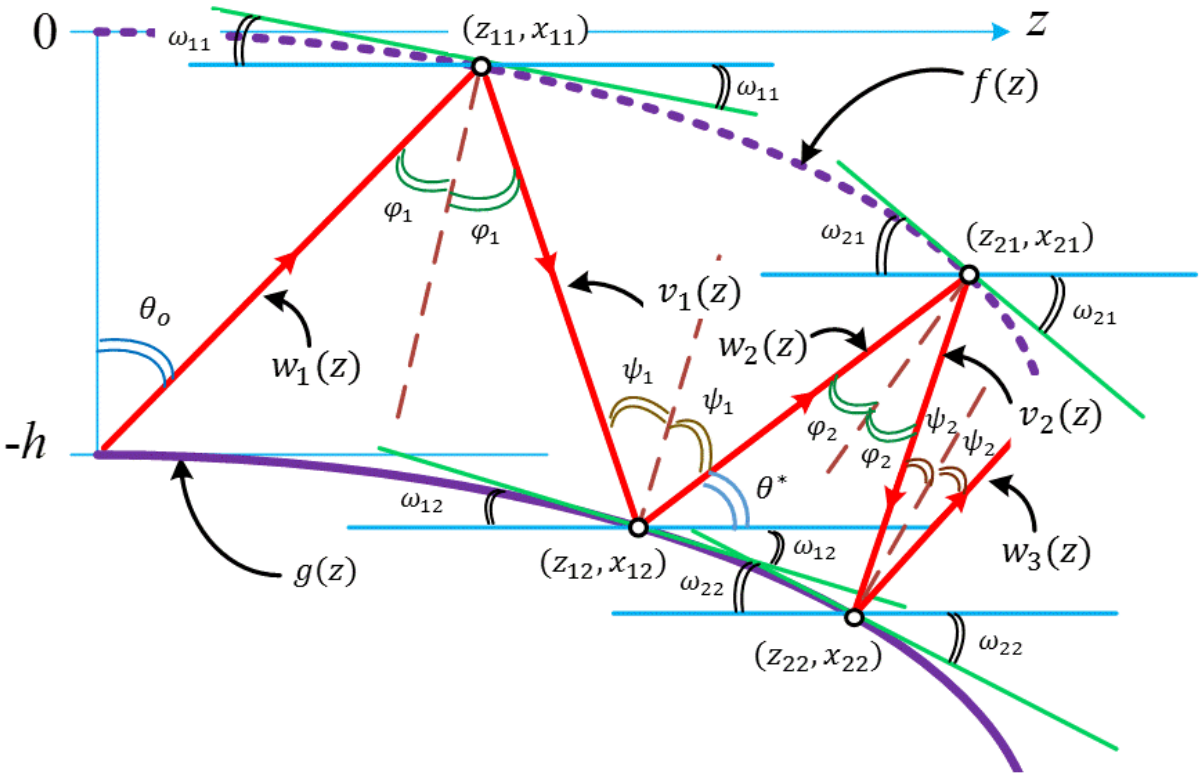

Figure 8. Extending the discrete ray tracing process.

Similar geometrical derivations are applied, except that now the leaky guide wall has an ogive curve and we also assume that the lower PEC wall can have an ogive curve with different parameter, namely:

$$g(z) = \sqrt{b^2 - z^2} - b - h \quad (18)$$

Notice that for larger diameter (lower curvature) of the PEC wall we need to have $b > a$, moreover, with very high parameter value ($b \gg 1$) the curve becomes almost horizontal.
The similar derivation for shape function is summarized in the following.

a. Determine the intersection of the ray specified by $w_1(z)$ and the leaky wall $f(z)$.

$$w_1(z) = \tan(90^o - \theta_o)\, z - h = \cot(\theta_o)\, z - h$$

$$f(z) = \sqrt{a^2 - z^2} - a$$

Solve for the nonlinear equation $\sqrt{a^2 - z^2} - a - \cot(\theta_o)\, z + h = 0$, which can be done by "fzero" function in Matlab to obtain z_{11}. And the corresponding coordinate

$$x_{11} = \cot(\theta_o)\, z_{11} - h$$

b. Compute the absolute of slope angle of $f(z)$ at the intersection point.

$$f'(z) = -\frac{z_{11}}{\sqrt{a^2 - z_{11}^2}}, \quad \omega_{11} = \tan^{-1}\left(-f'(z_{11})\right)$$

c. Find the equation of the reflected ray $v_1(z)$ as follows.

$$\varphi_1 = 90^o - (90^o - \theta_o) - \omega_{11} = \theta_o - \omega_{11}$$
$$m_{v_1} = -\tan(\omega_{11} + 90^o - \varphi_1) = -\tan(90^o - \theta_o + 2\omega_{11}) = -\cot(\theta_o - 2\omega_{11})$$
$$v_1(z) = -\cot(\theta_o - 2\omega_{11})\, z + x_{11} + \cot(\theta_o - 2\omega_{11})\, z_{11} \quad (19)$$

d. The intersection point (z_{12}, x_{12}) of the latter ray $v_1(z)$ and the lower side wall specified by $g(z)$ cannot be done because of the unknown parameter b in the lower side wall equation. If we had this intersection point the new absolute slope angle could be computed by

$$\omega_{12} = \left|\tan^{-1}\left(g'(z_{12})\right)\right| = \tan^{-1}\left(-g'(z_{12})\right) = \tan^{-1}\left(\frac{z_{12}}{\sqrt{b^2 - z_{12}^2}}\right) \quad (20)$$

But according to the same process that culminated in equation (13) we should require that the slope angle be equal such that the leaky wave be in parallel. That is $\omega_{12} = \omega_{11}$.

This requirement, in conjunction to equation (20) for known ω_{11}, can be used to compute the abscissa of intersection point z_{12}.

$$\omega_{12} = \omega_{11} = \tan^{-1}\left(\frac{z_{12}}{\sqrt{b^2 - z_{12}^2}}\right) \rightarrow \tan(\omega_{11}) = \frac{z_{12}}{\sqrt{b^2 - z_{12}^2}} \quad (21)$$

Solving the equation (21) for z_{12} with known value of ω_{11} we will have

$$z_{12} = b\sin(\omega_{11}) \quad (22)$$

Obviously $z_{12} = b\sin(\omega_{11}) > 0$ is guaranteed. The corresponding function value of this intersection point can also be found (after some algebra) in terms of unknown b as

$$x_{12} = g(z_{12}) = g(b\sin(\omega_{11})) = b(\cos(\omega_{11}) - 1) \quad (23)$$

Here we also see that $x_{12} = b(\cos(\omega_{11}) - 1) < 0$ because $\cos(\omega_{11}) - 1 < 0$ as we require for proper value of x ordinate.

e. Finally, the intersection point (z_{12}, x_{12}) that are computed in terms of b value must satisfy the equation of $v_1(z)$ in (19).

$$x_{12} = v_1(z_{12}) = -\cot(\theta_o - 2\omega_{11})\, z_{12} + x_{11} + \cot(\theta_o - 2\omega_{11})\, z_{11}$$
$$b(\cos(\omega_{11}) - 1) = -\cot(\theta_o - 2\omega_{11})\,(b\sin(\omega_{11})) + x_{11} + \cot(\theta_o - 2\omega_{11})\, z_{11}$$

Solving for unknown b value we have

$$b = \frac{x_{11} + \cot(\theta_o - 2\omega_{11}) + z_{11}}{\cos(\omega_{11}) + \sin(\omega_{11})\cot(\theta_o - 2\omega_{11}) - 1} \quad (24)$$

The computed value of b for this intersection point determines the main parameter of the ogive shape we approximate for the lower wall, or at least provide us with a point (z_{12}, x_{12}) on that wall that can be collected with further intersection point values.

f. The process outlined in the above steps must be repeated to obtain many points of intersection (z_{i2}, x_{i2}) for $i = 1, 2, 3, \ldots$ as shown in Figure 8 for two iterations. The collection of these

points can be used to determine the shape of the lower PEC side wall of the leaky guide. We will use a Matlab script to demonstrate this process.

g. Based on the derivations of the above steps, we can recognize a theoretical limit for the bend curvature depth beyond which the wave stops in the guide and behaves similar to the cutoff frequency. The slope of the partially reflected wave $v_i(z)$ from the leaky side must remain less than 90^o in absolute value for the TEM wave to move forward in the guide that is $90^o - \theta_o + 2\omega_{11} < 90^o$ (see equation (6) or the one before (19)).

$$-\theta_o + 2\omega_{11} < 0 \rightarrow \omega_{11} < \frac{\theta_o}{2}$$

Or generally for each reflection point

$$-\theta_o + 2\omega_{i1} < 0 \rightarrow \omega_{i1} < \frac{\theta_o}{2} \qquad (25)$$

But we know that $\theta_o = \cos^{-1}\left(\frac{f_c}{f}\right)$ and for any slope angle in the iterative computation we have $\omega_{i1} = \tan^{-1}\left(-f'(z_{i1})\right)$ with i being the index of the iteration step. Then using these relations we have

$$\cos^{-1}\left(\frac{f_c}{f}\right) > 2\tan^{-1}\left(-f'(z_{i1})\right) = 2\tan^{-1}\left(\frac{z_{i1}}{\sqrt{a^2 - z_{i1}^2}}\right)$$

Taking the cosine of the above equation, we have

$$\frac{f_c}{f} > \cos\left(2\tan^{-1}\left(\frac{z_{i1}}{\sqrt{a^2 - z_{i1}^2}}\right)\right) \qquad (26)$$

Now using the identity of $\cos(2\alpha) = \frac{1-\tan^2(\alpha)}{1+\tan^2(\alpha)}$ we proceed with the equation (26) as follows.

$$\cos\left(2\tan^{-1}\left(\frac{z_{i1}}{\sqrt{a^2 - z_{i1}^2}}\right)\right) = \frac{1 - \frac{z_{i1}^2}{a^2 - z_{i1}^2}}{1 + \frac{z_{i1}^2}{a^2 - z_{i1}^2}} = \frac{a^2 - 2z_{i1}^2}{a^2} \qquad (27)$$

The equation (26) and (27) gives us a limitation on the operating frequency in relation to the size or depth of curvature.

$$\frac{f_c}{f} > \frac{a^2 - 2z_{i1}^2}{a^2} \rightarrow f < f_c\left(\frac{a^2}{a^2 - z_{i1}^2}\right) \qquad (28)$$

Now if we use the maximum desirable value for z that is the length of leaky guide L and replace the ogive parameter (and the formula for the caliber) $a = d\left(C^2 + \frac{1}{4}\right) = \frac{4L^2+d^2}{4d}$ we can translate the frequency limitation in terms of the ogive length and diameter.

$$f < f_c\left(\frac{(4L^2+d^2)^2}{(4L^2+d^2)^2-16L^2d^2}\right) \rightarrow f < f_c\left(\frac{4L^2+d^2}{4L^2-d^2}\right)^2 \quad (29)$$

The following Matlab script performs this compensation technique for the ogive-shape wall.

```
% Script name: "Vp_test3.m"
% This script is used to demonstrate the methodology of finding the points
% on the lower side wall when the upper leaky wall id an ogive with the
% parameters in the script and the lower wall is approximated similarly.
%
%  Sam Jalali, SARA, Inc., Cypress, California
%  Version: 1.0,  11/05/2015
% ************************************************************************
close all; clear all;
format long; format compact;

L = 1.0;    % cone length
d = 3.0;    % cone base diameter
C = L/d;    % caliber
a = d*(C^2+1/4);
c_const = 2.99792458e8;
h = 165.1e-3;          % guide width in meters
fc = c_const/(2*h);    % cutoff fequency in GHz
f = 1.3e9;             % operating frequency
Teto = acos(fc/f);     % TEM modes angle
m1 = cot(Teto);

% Plot the complete upper side wall
z = linspace (0,L,200);
for n = 1:200
    x(n) = sqrt(a^2-z(n)^2)-a;
end
plot(z,x,':k','LineWidth',3.0); hold on;

mZ = 0; X = -h; Z = 0;
N = 10;                % number of reflections/iterations
z1(1) = 0; x1(1) = 0;
z2(1) = 0; x2(1) = -h;
w1(1) = 0;
% main loop
for n = 2:N
    % W2(n) = m1*z+x2(n)-m1*z2(n)
    % Compute the first intersection point, z11, x11
    fun1 = @ (z) sqrt(a^2-z^2)-m1*z-a-X+mZ;
    z1(n) = fzero(fun1,[Z,L]);
    x1(n) = m1*z1(n)+X-mZ;
    % x1(n) = sqrt(a^2-z1(n)^2)-a;     % alternative equation
    fpz1 = -z1(n)/sqrt(a^2-z1(n)^2);   % drivative value, f'(z1(n))
    w11 = atan(-fpz1);
    w1(n) = w11;                       % slope angle is stored to testing
    % Stop criterion check
    if w11 >= Teto/2
        break;
    end
    % Compute the second intersection point, z12, x12
    C1 = cot(Teto-2*w11); C2 = cos(w11); C3 =sin(w11);
    b(n) = (x1(n)+C1*z1(n)+h)/(C2+C3*C1-1);
    z2(n) = b(n)*sin(w11);
    x2(n) = b(n)*(cos(w11)-1)-h;
    mZ = m1*z2(n); X = x2(n); Z = z2(n);
end
% plot(z1,x1,':ms','LineWidth',3,'MarkerSize',4); hold on;
plot(z2,x2,'-ms','LineWidth',3,'MarkerSize',4); grid on;

for n = 1:4
    line([z2(n),z1(n+1)],[x2(n),x1(n+1)]);
    line([z1(n+1),z2(n+1)],[x1(n+1),x2(n+1)]);
end
```

The result of executing the above script, with some additions and observing the limitation discussed in part "g" above, is shown in Figure 9. Here the curvature is somewhat exaggerated for demonstration purposes. Practical curves are significantly smoother. The discussion in part "g" explains why the guided wave is not carried on past a certain z point. Appropriate parameters can be used for complete guide length simulation.

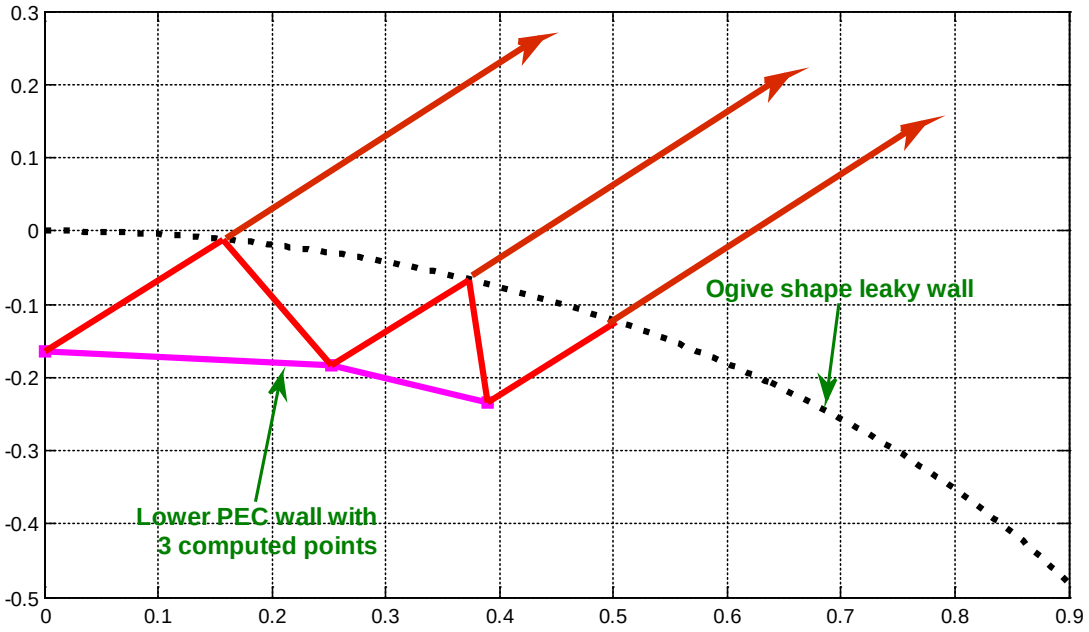

Figure 9. Employing extended phase velocity compensation.

3.5. Design approximation for the lower (PEC) wall of the LWA

In this section we attempt to develop and test an algorithm for computing grid wire diameters for an AAWSEA similar to what has been successfully done for the FAWSEA. Since the geometry of the AAWSEA makes the required steps for this part of project more complicated, we do not include a dielectric window initially.

The leaky wall of the assumed guide will be curved according to ogive shapes with zero offset as described in Section 3.3. Generally, for waveguide curvatures where the radius is greater than 20 times the wavelength, variations of important parameters such as wave-number are slow, and some appropriate approximations are justified. We will take advantage of that here, to simplify the algorithm, while leaving detailed verification to numerical models.

A mathematical analysis was proposed in section 3.4 in order to compensate for the AAWSEA curvature, such that an almost plane radiated wave can be achieved. As a result, several points on the lower PEC wall were considered. A study of these points did not reveal a simple analytical functional representation. Various interpolating polynomial functions are available through the standard numerical methods; unfortunately employing such a polynomial resulted in significant error in the slope of the tangent lines at the interpolating points.

Regarding the quest for a more appropriate approximation to the curve of the compensating PEC wall, it should be noted that these ogive curves can fit only one point perfectly (aside from the common starting point). The most significant errors occur towards the end of the LWA (see Figure 10).

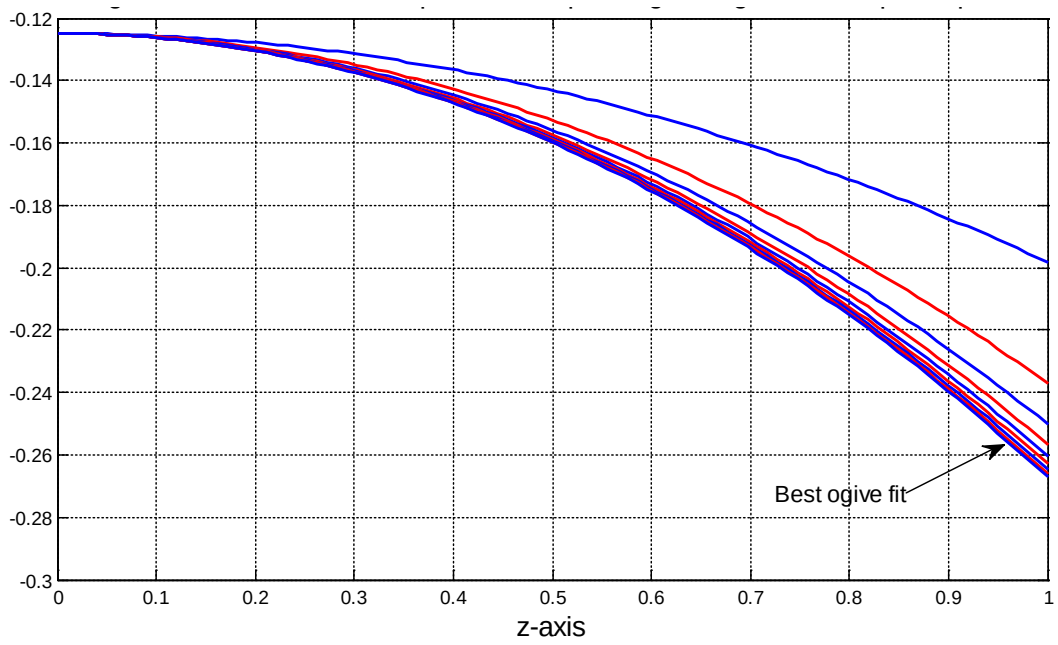

Figure 10. Ogive curves with different parameters, with a common starting point.

Three different alternatives were tested: A function created by interpolating a polynomial that passes through all the computed points seemed to be a natural option, however this function will have significant error in tangent line slopes at the interpolating points. The second option was an ogive curve with matching parameters for the end point of the LWA and the third was a simple quadratic function also compensating for the end point. A Matlab script was written to test the performance of these options. The script finds the reflection angles by solving for the intersection points as outlined in the previous section and shown in Figure 8. Studying the ogive approximation versus the quadratic one showed that the quadratic function performs better, with a maximum reflection angle error of 1.24 deg and minimum angle error of 0.23 deg, when the ogive curve fit had a maximum reflection angle error of 1.21 deg and minimum of 0.49 deg.

Figure 11 shows how closely the quadratic-fit curve for the lower PEC wall follows the computed points (the points are also shown). Here the leaky wall ogive function was selected for a guide of about 1 meter long, cone base diameter of 14 meters with the following formula. (Figure 11 indicates a short flat input section guide as well.)

$$f(z) = \sqrt{a^2 - z^2} - a, \qquad a = 3.5714286 \qquad (30)$$

The compensation achieved by the quadratic approximation $g(z) = C_o z^2 - h$ can be seen in Figure 12 where the plane wave radiation is predicted. As a conclusion, we simplify the complete analysis of AAWSEA used for determining the grid wire diameters by assuming perfect compensation for reflection angle and similarly for phase velocity. The latter is an important assumption, which not only eliminates complicated angle computations as outlined in the previous section but also will be applied in some other parameter calculations as will be explained in the following sections. Symbolically we refer to this assumption by $\theta_i = \theta_o$ for $i = 1, 2, \ldots$

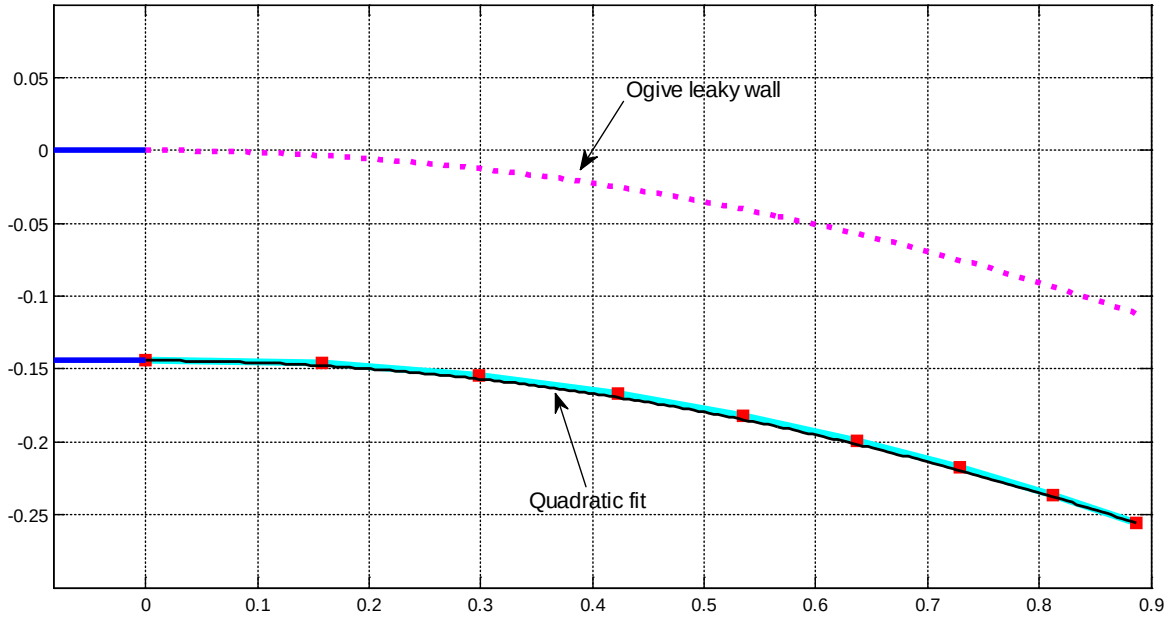

Figure 11. Use of a quadratic fit curve for the back wall.

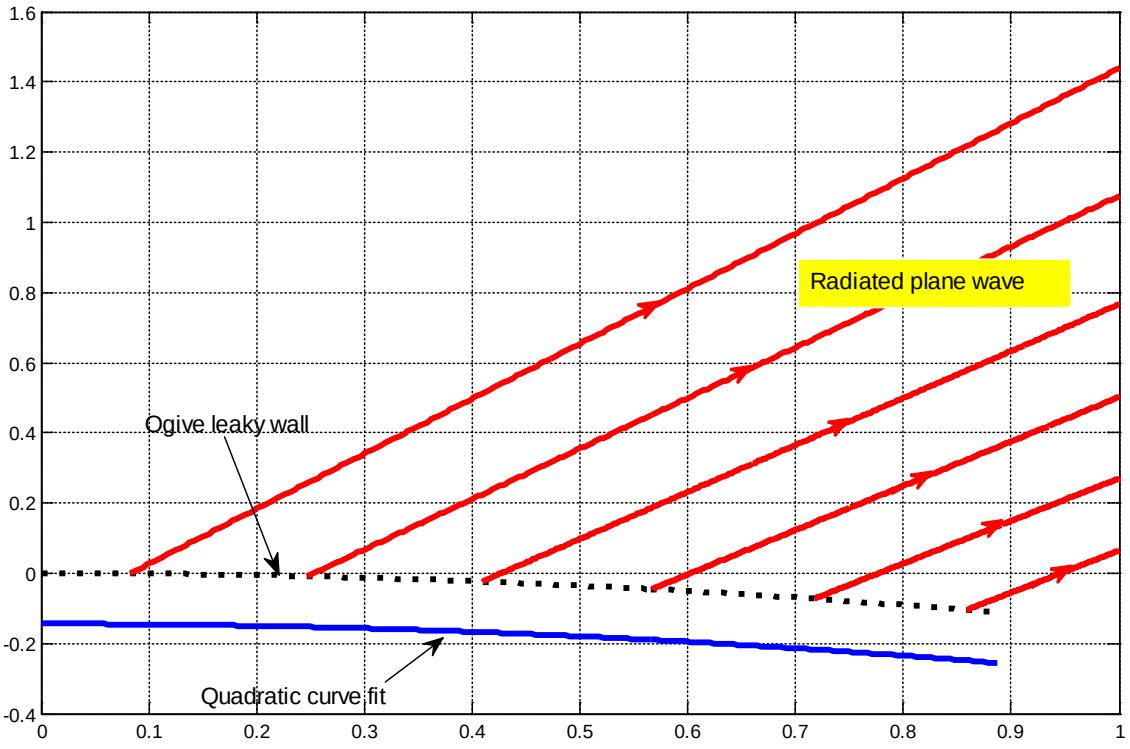

Figure 12. Predicted rays, radiated plane wave.

3.6. Mapping from flat axis to the arched line

A FAWSEA possesses a flat leaky wall along the z-axis. After introducing an arch, according to an ogive, we have the configuration known as an AAWSEA (Figure 13).

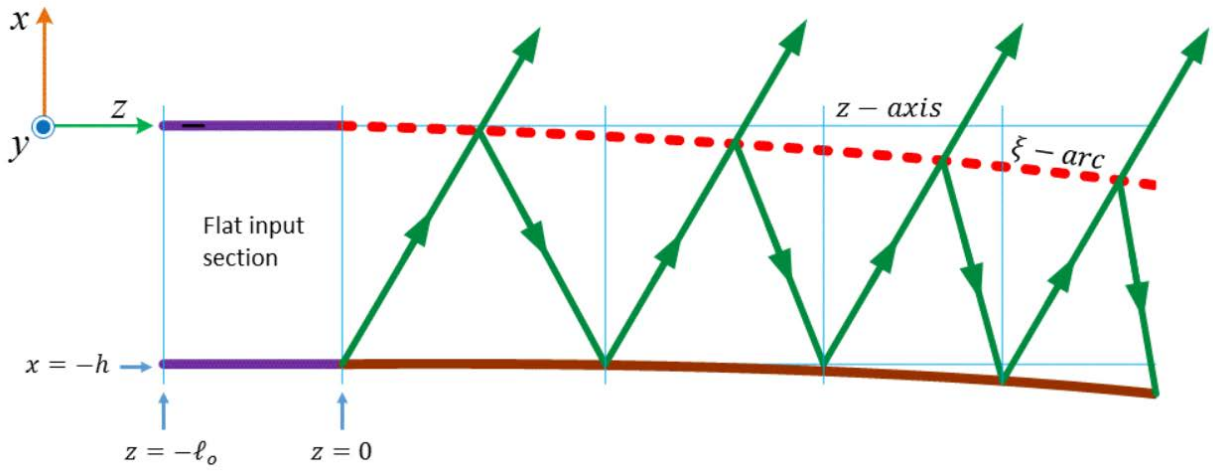

Figure 13. Predicted rays, arched configuration

Let us calculate the arc length denoted by $\xi = f(z)$ on the arched wall specified by the equation (30). By doing this calculation each point on the z-axis can be mapped to a corresponding point on the arched wall.

$$\xi = \int_0^z d\xi = \int_0^z \sqrt{dz^2 + dx^2} = \int_0^z \sqrt{1 + \left(\frac{dx}{dz}\right)^2}\, dz = \int_0^z \sqrt{1 + [f'(z)]^2}\, dz$$

$$f'(z) = -\frac{z}{\sqrt{a^2 - z^2}}, \qquad 1 + [f'(z)]^2 = \frac{a^2}{a^2 - z^2}$$

$$\xi = \int_0^z \frac{a}{\sqrt{a^2 - \zeta^2}}\, d\zeta = \mathrm{a}\sin^{-1}\left(\frac{\zeta}{a}\right)\Big|_0^z = a\sin^{-1}\left(\frac{z}{a}\right) \qquad (31)$$

With the conversion from the z-axis to the arc length, the reverse conversion is also known.

$$z = a\sin\left(\frac{\xi}{a}\right) \qquad (32)$$

3.6.1. Wave leakage rate on the arched wire grid

An ideal attenuation rate that represents the wave leakage from the guide was formulated for FAWSEA previously (e.g., see the 1st Quarterly Report). This attenuation rate, which varies with distance along the guide, has been proved to be successful and can be generalized for AAWSEA. The ideal attenuation and its conversion to the arc-variable are given in the following equation.

$$\alpha_{ideal}(z) = \frac{1}{L - z}, \qquad \alpha_{ideal}(\xi) = \frac{1}{L - a\sin\left(\frac{\xi}{a}\right)} \qquad (33)$$

3.7. Ideal power reflection coefficient

Another important formalism successfully tested in analysis of FAWSEA antenna is related to derivations of the ideal power reflection along the guide based on the first order differential equation formulation.

$$R_{P,Ideal}(z) = \exp(-S\alpha_{ideal}(z)) \qquad (34)$$

In the above equation S represents the distance between consecutive intersections of plane wave rays on the grid, and is constant for FAWSEA.

$$S_o = \frac{4h^2}{\lambda_g} = \frac{4h^2 \sin\theta_o}{\lambda_o} \qquad (35)$$

In equation (35) the θ_o is the complement of the desired radiation angle and h is the guide width, per Figure 14.

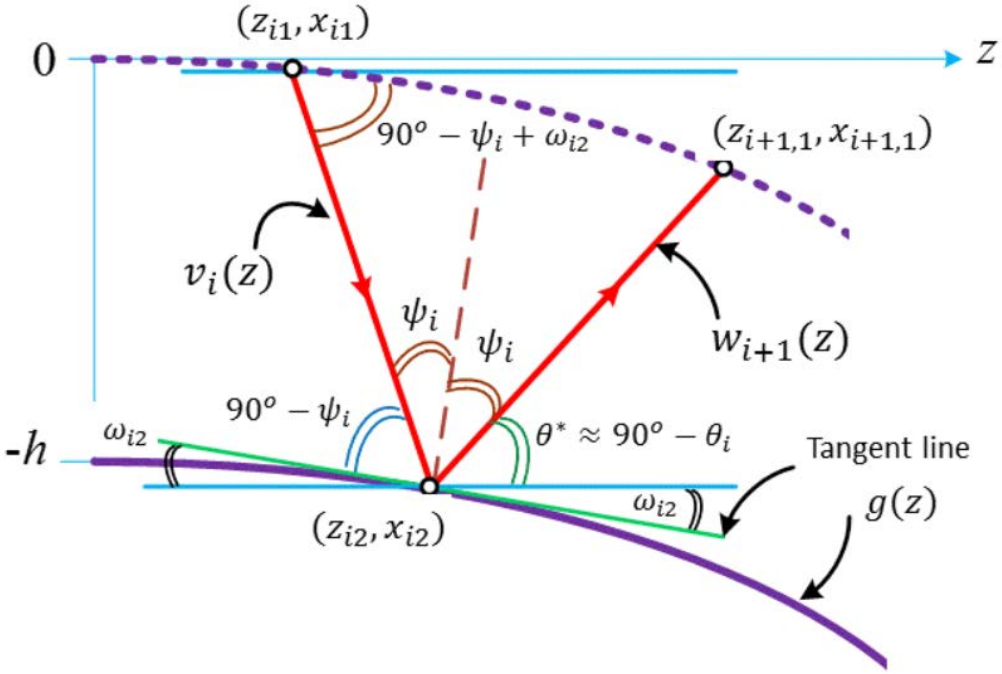

Figure 14. Detail of ray tracing between points.

This parameter h is no longer constant, in contrast to the flat aperture case (FAWSEA). It will vary from point to point along the guide as seen in Figure 13. First, notice that we require a minimum of flat input section (no leakage) for the guide that is determined by $\ell_o = h\tan\theta_o$ for proper injection of the wave into the leaky guide. Now in order to achieve a good estimate of this length denoted by S_i we can compute the successive intersecting points of the rays inside the guide as shown by points (z_{i1}, x_{i1}) and $(z_{i+1,1}, x_{i+1,1})$, and the approximation for S_i is done by computing the straight distance between these points, as in:

$$S_i = \sqrt{(z_{i+1,1} - z_{i1})^2 + (x_{i+1,1} - x_{i1})^2} \qquad (36)$$

The concise methodology used to compute these points is summarized in the following.

- The equation for the leaky wall $f(z) = \sqrt{a^2 - z^2} - a$ and the PEC (lower) wall $g(z) = C_o z^2 - h$ are known.

- We will place the grid wires at equal distance on the arched wall denoted by ξ_i for $i = 1, 2, \ldots$
- For each location on the arched wall ξ_i we compute the starting point $(z_{i+1,1}, x_{i+1,1})$.
- Using the equation for the plane wave ray $w_{i+1}(z) = m_w(z - z_{i+1,1}) + x_{i+1,1}$ when $m_w = \cot\theta_i = \cot\theta_o$ and $g(z) = C_o z^2 - h$ is known, find the intersection point (z_{i2}, x_{i2}).
- Using the equation for the plane wave ray $v_i(z) = m_v(z - z_{i,2}) + x_{i,2}$ when $m_v = -\cot(\theta_i - 2\omega_{i2}) = \cot(\theta_o - 2\omega_{i2})$, $\omega_{i2} = |\tan^{-1}(2C_o z_{i2})|$ and $f(z)$, find the intersection point (z_{i1}, x_{i1}).
- Finally use equation (36) to estimate the value S_i for this point.

Unfortunately the above procedure can only be applied when the location of the grid wire is appropriately inside the guide. That is when $\xi_i \geq \xi_2$ in Figure 15. When the arc length is smaller than ξ_2 we have to estimate the S_i in a different way. When $\xi_1 < \xi_i \leq \xi_2$ we need to use a modified procedure, and finally when $\xi_i < \xi_1$, yet another modified process has to be employed.

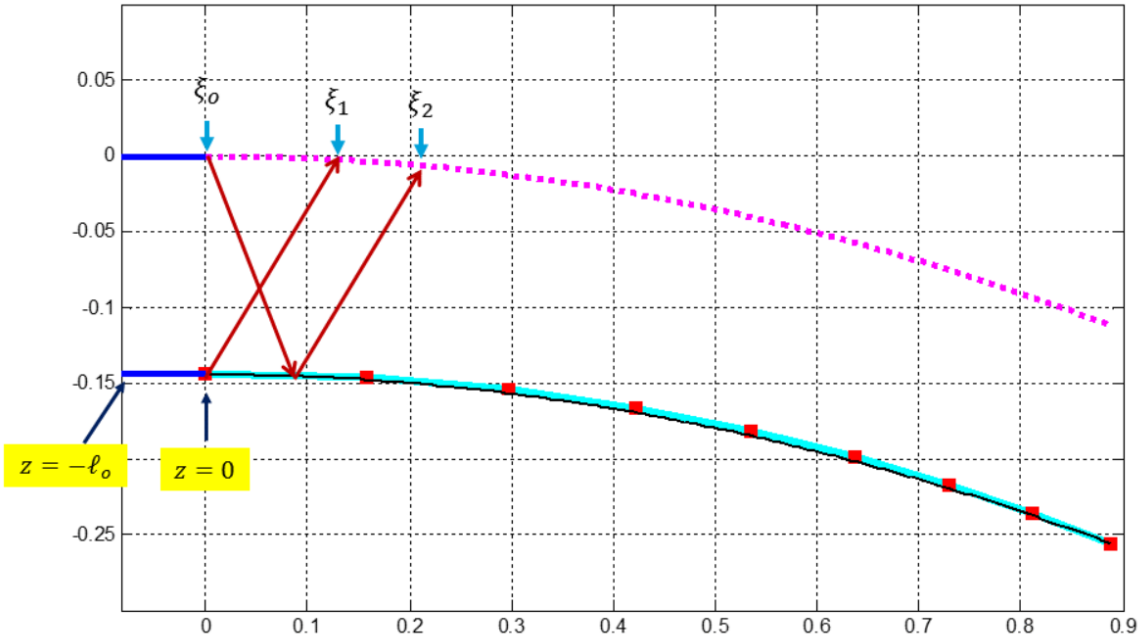

Figure 15. Points used in the methodology

3.8. Computing the variable angle of incidence for use in Marcuvitz's equation

In order to compute the grid wire diameters, we use a similar methodology as before, requiring the equivalence of the ideal power reflection and the one resulting from the Marcuvitz formula for infinite parallel wire grids (see our 1st Quarterly Report). The process is summarized as follows.

- The ideal power reflection for each wire location on the arched leaky wall is now computed as follows (now using the computed S_i).

$$R_{P,Ideal}(\xi_i) = \exp(-S_i \alpha(\xi_i)) \qquad (37)$$

- We also need to compute the power reflection using the generic formula $R_{Pow} = |\Gamma|^2$ where $\Gamma = (Z_{eq} - 1)/(Z_{eq} + 1)$ is the equivalent circuit reflection coefficient. The formula given by Marcuvitz (described previously) needs to be iteratively computed. The only difference in the case of AAWSEA compared to FAWSEA is that the angle of incidence considered in Marcuvitz is no longer constant, varying with the location of the grid wire in the leaky wall. Figure 16 shows the variation of this angle denoted by $\varphi_1, \varphi_2, \ldots$ in the figure. When the angle φ_i for each wire location is computed, the power reflection can be calculated using a similar Matlab function.
- It was shown in section 3.4 (via geometric derivations) that $\varphi_i = \theta_i - \omega_{i1}$. Now, employing the perfect compensation assumption $\theta_i = \theta_o$ for $i = 1, 2, \ldots$ that will become $\varphi_i = \theta_o - \omega_{i1}$
- The required angle ω_{i1} for each point on the arched wall ξ_i is easily computed as follows.

$$\omega_{i1} = |\tan^{-1} f'(z_{i1})| = \tan^{-1}\left(\frac{z_{i1}}{\sqrt{a^2 - z_{i1}^2}}\right) \qquad (38)$$

Now substituting $z_{i1} = a \sin\left(\frac{\xi_i}{a}\right)$ in equation (38) we proceed as in

$$\omega_{i1} = \tan^{-1}\left(\frac{a \sin\left(\frac{\xi_i}{a}\right)}{a\sqrt{1 - \sin^2\left(\frac{\xi_i}{a}\right)}}\right) = \tan^{-1}\left(\tan\left(\frac{\xi_i}{a}\right)\right) = \frac{\xi_i}{a} \qquad (39)$$

Finally, we have

$$\varphi_i = \theta_o - \frac{\xi_i}{a} \qquad (40)$$

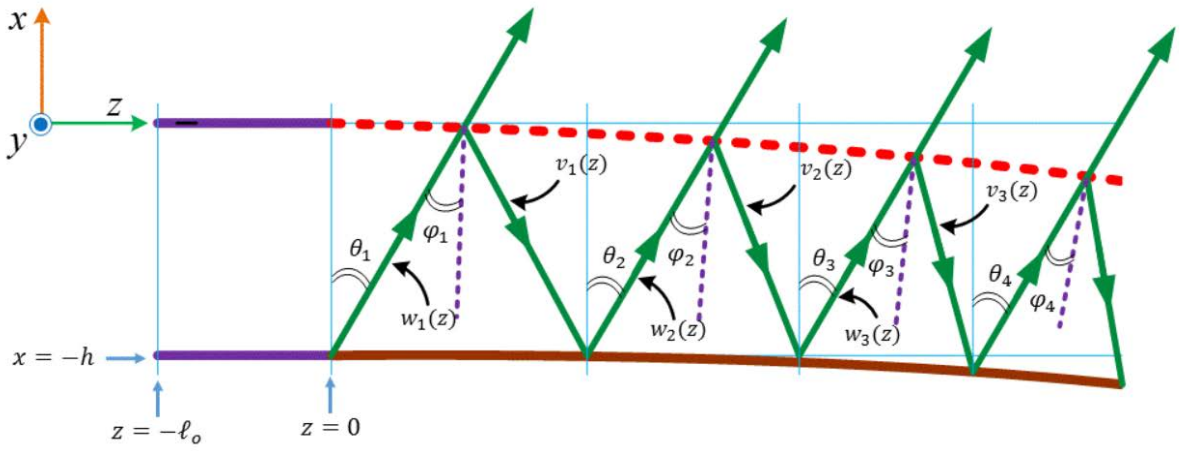

Figure 16. Variation of angle of incidence on the leaky wall.

The above analyses establish most of the framework needed for an (approximate) AAWSEA design theory, to be tested against numerical models. We are currently preparing Matlab scripts and functions that incorporate these expressions, and which will allow us to explicitly compute the wire sizes and spacings that ought to go with the subject H-plane curved boundaries. The next steps will be to compare the predicted wire grill configurations, VSWR, and antenna patterns of candidate AAWSEA configurations to our more established FAWSEA configurations, initially in 2D, and ultimately in 3D models that include dielectric windows and multiple, parallel, finite-width channels.

4. DISCUSSION, CONCLUSIONS, AND RECOMMENDATIONS

Research performed during this 9th quarter of the R&D program focused upon developing a theoretical framework/toolset to help guide the AAWSEA "design recipe" process, proceeding in analogy to the theory and tools we established previously to guide the design of FAWSEAs and CAWSEAs. To that end, we endeavored to expand the plane-wave decomposition perspective into a more general, but also more-approximate, ray-tracing technique. More work is needed to advance and validate this analysis, identify its limitations, and to establish its effectiveness in accelerating the AAWSEA design process, which (until now) has been based mostly on geometrically morphing FAWSEA designs and then re-tuning them by means of computationally-intensive iterative numerical modeling.

In the coming quarter, we plan to: (1) complete the investigation (and validation, if all goes well) of the generalized ray tracing approach (in combination with the previously-established tools) to formulating AAWSEA design recipes; and (2) make significant progress toward optimization and documentation of "standard/ recommended" designs for AAWSEA, BAWSEA, and RAWSEA.

As always, we appreciate ONR's continuing support for this R&D.

BIBLIOGRAPHY (alphabetical)

Bodnar, D.G. and D.T. Paris, “New Variational Principle in Electromagnetics,” *IEEE Trans. Antennas & Propagat*, vol. AP-18, pp. 216-223, 1970

Goldstone, L.O. and Oliner, A.A., “Leaky-Wave Antennas I: Rectangular Waveguides," *IRE Trans. Ant. and Propagat*., Oct., 1959, pp. 307-319.

Goldstone, L.O. and Oliner, A.A., “Leaky-Wave Antennas II: Circular Waveguides," *IRE Trans. Ant. and Propagat*., May., 1961, pp. 280-290.

Honey, R.C., “A Flush-Mounted Leaky-Wave Antenna with Predictable Patterns,” *IRE Trans. Antennas and Propagat*., 7, pp. 320-329, 1959.

Ishimaru, A.K. and Beich, F.R., “Pattern Synthesis With a Flush-Mounted LeakyWave Antenna on a Conducting Circular Cylinder,” *J. of Res. of the Nat. Bureau of Standards-D. Radio Propagat* Vol. 66D, No.6, Nov- Dec. 1962, pp. 783-796.

Jull, E.V., “Radiation from Apertures,” Chap. 5 of *Antenna Handbook: Theory, Applications, and Design*, Ed. by Y.T. Lo and S.W. Lee, Van Nostrand Reinhold, NY, 1988.

Lewin, L., “Theoretical analysis of the junction discontinuity between a straight and a curved section of rectangular waveguide,” *Proc. IEE,* Vol. 124, pp. 511-516, 1977.

Lewin, L., “The E-plane Taper Junction in Rectangular Waveguide,” *IEEE Trans. Microwave Theory and Techniques*, vol. MTT-27, pp. 560-563, 1979.

Marcuvitz, N., *Waveguide Handbook*, McGraw-Hill, NY, 1951.

Nishida, S., “Coupled Leaky Waveguides I: Two Parallel Slits in a Plane” *IRE Trans. Ant. and Propagat*., May, 1960, pp. 323-330.

Nishida, S., “Coupled Leaky Waveguides II: Two Parallel Slits in a Cylinder,” *IRE Trans. Ant. and Propagat.*, July, 1960, pp. 354-360.

Oliner, A.A. and R.G. Malech, “Radiating Elements and Mutual Coupling,” “Mutual Coupling in Infinite Scanning Arrays,” and “Mutual Coupling in Finite Scanning Arrays,” -- Chaps. 2, 3, and 4 respectively of *Array Theory and Practice*, Vol. II of *Microwave Scanning Antennas*, Ed. by R.C. Hansen, Peninsula Publishing, Los Altos, CA, 1985.

Oliner., A.A, and D.R. Jackson, “Leaky Wave Antennas," Chap. 11 of *Antenna Engineering Handbook*, 4th Ed., Edited by J.L. Volakis, McGraw-Hill, NY, 2007.

Schwinger, J., and D.S. Saxon, *Discontinuities In Waveguides - Notes on Lectures by Julian Schwinger*, Gordon and Breach Science Publishers, NY, 1968.

Silver, S., *Microwave Antenna Theory and Design*, 1st Ed, publ. by office of Scientific Research and Development, National Defense Research Committee, NY, 1949.

SUGGESTED DISTRIBUTION LIST

Official Record Copy
Mr. Lee Mastroianni
E-Mail: lee.mastroianni@navy.mil
Code 30
Office of Naval Research
875 North Randolph St.
Arlington, VA 22203-1995 1 cy

Dr. Joong H. Kim
E-Mail: joong.kim@navy.mil
Code 30
Office of Naval Research
875 North Randolph St.
Arlington, VA 22203-1995 1 cy

Director, Naval Research Lab
E-mail: reports@library.nrl.navy.mil
Attn: Code 5596
4555 Overlook Avenue, SW
Washington, D.C. 20375-5320 1 cy

Defense Technical Information Center
E-mail: tr@dtic.mil
8725 John J. Kingman Road
STE 0944
Ft. Belvoir, VA 22060-6218 1 cy

Dr. Donald Shiffler
AFRL/RDH
Kirtland AFB, NM 87117-5776 1 cy

Dr. Kyle Hendricks
AFRL/RDHP
Kirtland AFB, NM 87117-5776 1 cy

Dr. Andrew D. Greenwood
AFRL/RDHE
Kirtland AFB, NM 87117-5776 1 cy

Dr. Susan Heidger
AFRL/RDH
Kirtland AFB, NM 87117-5776 1 cy

Mr. Matthew McQuage
Naval Surface Warfare Center
Dahlgren Division, Q07
Dahlgren, VA 22448 1 cy

Michael Wagaman
Advanced Technology Directorate
PEO Strike Weapons and Unmanned Aviation
Patuxent River, MD. 1 cy

Dr. Frank E. Peterkin
Director
Directed Energy Technology Office
17320 Dahlgren Road
Naval Surface Warfare Center
Dahlgren, VA 22448 1 cy

LTC Charles Ormsby
Chief
Directed Energy Requirements
Langley AFB, VA 1 cy

Patrick Randeson
Science, Technology and Weapons Analyst
Central Intelligence Agency
Washington, D.C. 1 cy